ORIGINAL ARTICLE

Influence of cutting edge radius on surface integrity and burr formation in milling titanium

Carl-Frederik Wyen · Dominik Jaeger · Konrad Wegener

Abstract The influence of the cutting edge micro geometry on cutting process and on tool performance is subject to several research projects. Recently, published papers mainly focus on the cutting edge rounding and its influence on tool life and cutting forces. For applications even more important, however, is the influence of the cutting edge radius on the integrity of the machined part. Especially for titanium, which is used in environments requiring high mechanical integrity, the information about the dependency of surface integrity on cutting edge geometry is important. This paper therefore studies the influence of the cutting edge radius on surface integrity in terms of residual stress, micro hardness, surface roughness and optical characterisation of the surface and near surface area in up and down milling of the titanium alloy Ti–6Al–4V. Moreover, the influence of the cutting edge radius on burr formation is analysed. The experiments show that residual stresses increase with the cutting edge radius especially in up milling, whereas the influence in down milling is less pronounced. The influence of the cutting edge radius on surface roughness is non-uniform. The formation of burr increases with increasing cutting edge radius, and is thus in agreement with the residual stress tests.

Keywords Cutting edge radius · Surface integrity · Burr formation · Milling · Titanium

C.-F. Wyen (✉)
Rieter Machine Works Ltd.,
Winterthur, Switzerland
e-mail: carl-frederik.wyen@rieter.com

D. Jaeger
Laboratory for Nanoscale Material Science, EMPA,
Duebendorf, Switzerland

C.-F. Wyen · K. Wegener
Institute of Machine Tools and Manufacturing (IWF), ETH Zurich,
Zurich, Switzerland

Symbols and acronyms

a_e	Width of cut
a_p	Depth of cut
d	Diameter
f_z	Feed per tooth
$h_{(min)}$	(Minimum) uncut chip thickness
n	Number of cutting edges
p	Pressure
r_n	Cutting edge radius
t	Thickness
t_i	Indentation time
v_c	Cutting velocity
v_f	Feed speed
F	Force
I	Current
HV	Vickers Hardness
$Ra_{(t)}$	(Theoretical) arithmetic mean roughness
$Rz_{(t)}$	(Theoretical) kinematic surface roughness
U	Voltage
α	Clearance angle
γ	Rake angle
θ	Half diffraction angle
λ	Wave length
λ	Cutoff frequency
μ	Coefficient of friction
ρ	Friction angle
σ	Residual stress
φ	XRD measurement direction
ψ	Incident angle

1 Introduction

Rounded cutting edges are known to positively influence tool performance in several machining processes. The radius of a cutting edge affects the stability of the edge [1, 2], the

forces occurring on the cutting edge [3, 4] and the cutting temperature [5]. Besides having an impact on tool life time [1, 6–8], the edge radius also influences the surface state of the machined workpiece, also referred to as surface integrity [9–17]. Broadly, surface integrity is defined as the metallurgical, mechanical, topographic and chemical state of the machined surface [18].

The surface state may significantly influence the mechanical properties and thus the fatigue life of a component. It is therefore important to not only know the influence of rounded cutting edges on tool performance but, and for the product even more important, also the influence on the surface state. Surface integrity is generally assessed using microhardness measurements, residual stress measurements or microstructural analyses which reveal microcracks, phase transformations, melted and redeposited layers or similar features [19, 20].

Further economically important to know is how the cutting edge geometry influences the formation of burr. Burr results from deformation of material in the near surface area. It is therefore closely related to the impact of the cutting edge geometry on surface integrity. Burr is generally undesirable. It has a negative impact on tool wear as it can cause strong abrasive groove wear when hitting the cutting edge. Due to its sharpness, burr is potentially dangerous for operators handling workpieces. Burr also hinders subsequent assembly operations. Therefore, burr generally needs to be removed in subsequent deburring operations.

The fact that titanium is typically used in applications which require high workpiece integrity makes it even more important for this material to identify the impact of the edge micro geometry on surface integrity. For the milling of titanium, no such information is available yet. For this reason, this paper experimentally analyses the influence of the cutting edge geometry on surface integrity and also burr formation in milling the titanium alloy Ti–6Al–4V.

2 Experimental setup and procedure

To evaluate the influence of the cutting edge micro geometry on surface integrity in milling Ti–6Al–4V, tests were accomplished on a Mikron VC1000 3-axis machining centre. The chemical composition of the work material is given in Table 1. The machining setup is illustrated in Fig. 1.

An 8 % Motorex Swisscool Magnum UX 200 emulsion was used as coolant, which was supplied externally and

Table 1 Chemical composition of Ti–6Al–4V

Element	Fe	Al	V	O	C	N	Ti
Content (wt%)	0.19	6.27	4.01	0.18	0.002	0.005	Remainder

through the tool at a pump pressure of $p=40$ bar. The surfaces were generated in a free orthogonal slot milling process, meaning that the corner was not engaged. The tests were carried out using a cutting speed of $v_c=70$ m/min, a feed per tooth of $f_z=0.08$ mm and a cutting width of $a_e=d=25$ mm. The cutting depth a_p was given by the sheet thickness of $t=4$ mm. The machining parameters correspond to values typically used in the machining of titanium. To keep dynamic effects low and to eliminate influences of simultaneous edge engagement and disengagement, the tool was equipped with one insert only. In slot milling, the main cutting edge generates two surfaces of which one is produced by up milling and the other one by down milling. In up milling, the cutter enters the cut at a minimum chip thickness, whereas in down milling the tool disengages the cut at a minimum chip thickness. This difference in kinematics is expected to influence the surface properties. Therefore, the analyses were performed for both generated surfaces of the titanium sheet.

The cutting edges were made of medium grain-sized straight cemented carbide. The cutting edge roundings were generated by edge-focused micro abrasive jet machining using a six-axis robot to guide the jet nozzle. The process is presented in [21]. The cutting edge radius was varied between $r_n=6\pm2$ μm (not jet treated after grinding) and $r_n=50\pm1$ μm, which represents a range typical for rounded cutting edges. The edges had a rake angle of $\gamma=10°$ and a clearance angle of $\alpha=8°$. The cutting edges were characterised using the method proposed in [22]. The inserts and tool holder were specially manufactured for the experiments.
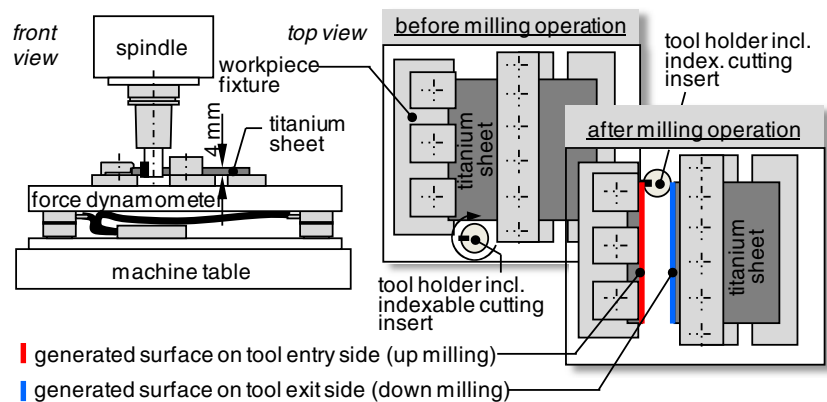
3 Measuring equipment

Macroscopic residual stresses were analysed using a Siemens Bruker D5000 X-ray diffractometer. The stresses were determined by the $\sin^2\psi$ method. The method is based on the determination of elastic lattice strains which are converted to stresses by the 3D form of Hooke's law [23, 24]. Macrostresses cause a distortion of the crystal lattice, which results in an angular shift of the diffraction peak selected for residual stress measurement. As the X-ray beam penetrates only to depths of approximately 5 μm, those measurements give information on the residual stress in a very shallow surface zone [25].

Peaks at large diffraction angles react more sensitive to stresses [26]. For that reason, strains were measured from the {213} lattice plane, which corresponds to a peak position of $2\theta_0=141.7°$ when using Cu Kα radiation ($\lambda=0.154$ nm) [25]. Furthermore, this peak gives a good signal to noise ratio and is not superimposed by other peaks. An overview of diffraction peaks detected when irradiating the Ti–6Al–4V sheet material with Cu Kα radiation is given in Fig. 2.

Fig. 1 Schematic of setup used for free orthogonal milling of titanium sheets

■ generated surface on tool entry side (up milling)

■ generated surface on tool exit side (down milling)

The peak shift was determined at ten incident angles in minimum, in a range of at least $-51.3° < \psi < 18.2°$. Measurements were performed in two directions longitudinal and lateral to the cutting directions ($\varphi = 0°, 90°$). All measurements were performed at a tube voltage of $U = 40$ kV and a tube current of $I = 35$ mA. A nickel filter in combination with a 1-mm divergence, a 1-mm anti-scatter and a 0.1-mm detector slit was used as focus setup.

Microhardness measurements were carried out according to DIN EN ISO 14577 using a *Fischerscope HM2000*. The instrument allows indentations with forces between 0.4 and 2000 mN and has a force uncertainty of 40 μN.

The microstructural analysis of the surfaces was carried out using a *Carl Zeiss DSM962* scanning electron microscope (SEM). Polished and etched cross sections were analysed using an *Alicona InfiniteFocus* microscope.

Surface roughness measurements were performed with the *Form Talysurf Series 2* surface profiler from *Taylor Hobson Ltd.* The surface profiler is equipped with a diamond stylus having a tip diameter of $d = 2.5$ μm. The surface profiles were evaluated using the *Taylor Hobson* software *Ultra v4.6.* The arithmetical mean roughness Ra and the ten point mean roughness Rz were determined according to [27] using a
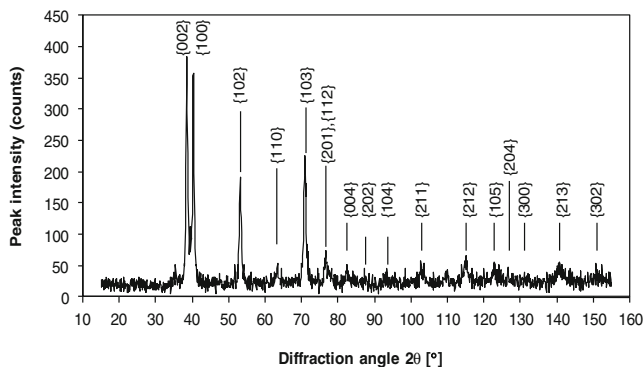
cutoff frequency of $\lambda_c = 0.8$ mm. Burr was observed using an optical *Leica MZ16 A* microscope.

4 Experimental results

The following paragraphs evaluate and discuss the influence of the cutting edge radius on surface integrity by means of residual stress measurements, micro hardness measurements, SEM surface analyses, roughness measurements and texture examination of polished and etched cross sections. Moreover, the influence of rounded cutting edges on burr formation is discussed. For all parameters determined experimentally and depicted in diagrams, the actually observed error including measurement uncertainty is given by the error bars.

4.1 Residual stress

Residual stress is generally caused by mechanical and thermal loads. Mechanical loads induce compressive stresses, whereas thermal loads cause tensile stresses. In machining, material is plastically deformed until material failure occurs in front of the cutting edge, separating the chip from the workpiece. The deformation and failure process is strongly influenced by the tool geometry and process kinematics [28].

The cutting edge radius influences the forces in the cutting process. The force that acts directly on the cutting edge is also referred to as ploughing force [29].

It is thus the force which also directly influences the surface being generated. With increasing cutting edge radius, especially the feed force component of the ploughing force increases [3]. This indicates that an additional material deformation in front of the cutting edge, respectively between the cutting edge and surface being generated, occurs, which consequently generates compressive stresses. Hence, an increase in mechanical deformation and thus compressive residual stress with increasing cutting edge radius can be expected for both processes up and down milling. Compressive residual

Fig. 2 Diffraction peaks and corresponding lattice planes {hkl} of Ti–6Al–4V detected using Cu Kα radiation; lattice plane mapping accordant to [45, 46]

stresses are favourable as they improve workpiece fatigue strength and resistance to stress corrosion cracking [28].

Plastic deformation involves the generation of heat. With increasing deformation, caused by a larger cutting edge radius, it is thus to expect that cutting temperatures increase. Furthermore, the contact area and thus frictional area increases with increasing cutting edge radius. Investigations made by [5], however, have shown that in turning steel cutting temperatures increase by less than 1 °C per μm increase in cutting edge radius.

In up milling, the uncut chip thickness increases within the cut. Before chip formation occurs, a friction and material compression process starts, inducing elastic–plastic deformation into the workpiece surface [30]. The affected area—cutting edge entry until minimum chip thickness is reached—increases with increasing cutting edge radius as the minimum chip thickness is influenced by the cutting edge radius [31]. The larger the radius, the higher are the forces on the surface to be generated. At cutting edge entry, the edge temperature is assumed to be low. The generated surface is thus expected to be mostly influenced by mechanical induced compression processes.

In down milling, however, the tool exit condition is characterised by a continuously decreasing chip thickness until no cutting action occurs due to under-running the minimum chip thickness. The properties of the generated surface are mainly determined by the separation processes involved in chip formation [30]. Moreover, tool temperature in down milling can be expected to have a higher effect on residual stress as the edge which is in contact with the new surface is heated up by the foregoing cutting action.

Caused by elastic deflections, the newly generated surface might be compressed again when being in contact with the cutting edge during the following tool rotation. The area which is repeatedly in contact with the rotating cutting edge depends on system stiffness, tool diameter and feed rate.

Figure 3 shows the results of residual stress measurements on surfaces generated in up milling (left) and down milling (right) with different cutting edge radii. The angle φ denotes the measurement direction in residual stress analysis. An angle of $\varphi=0°$ denotes measurements in the direction of cutting, whereas $\varphi=90°$ stands for measurements orthogonal to the direction of cutting. The directions of feed and cutting speed were parallel to each other at tool entry and exit.

Polished reference samples showed an average residual stress of $\sigma=12$ N/mm^2. Both up and down milling induce residual stresses of compressive type. The compressive stresses measured in the direction orthogonal to the cutting velocity are generally higher than those determined in the direction of cutting, which is in agreement with residual stress measurements made by [30, 32].

In up milling, the maximum induced residual compressive stresses on the surface increase with increasing cutting edge radius from around $\sigma=-310$ N/mm^2 when using a non-rounded cutting edge ($r_n\approx6\pm2$ μm) to approximately $\sigma=-600$ N/mm^2 when machining with edges rounded to a radius of $r_n=50\pm1$ μm. Including measurement uncertainty, the scattering of residual stresses averages ±32 N/mm^2 for machined surfaces.

In down milling, the maximum detected compressive stresses react less sensitive to a change in cutting edge radius. Compressive stresses on the surface remain roughly at an average value of $\sigma=-400$ N/mm^2. This behaviour might be caused by opposite effects of mechanical and thermal load when using rounded cutting edges. The mechanical deformation increases with increasing cutting edge radius, causing a specific elastic–plastic deformation on the machined surface. At the same time, process temperatures increase, which shift the surface stress towards the tensile direction. Especially in the machining of titanium, known for its poor thermal conductivity that causes high temperatures which effect only

Fig. 3 Residual stress measured on Ti–6Al–4V surfaces machined with different cutting edge radii r_n
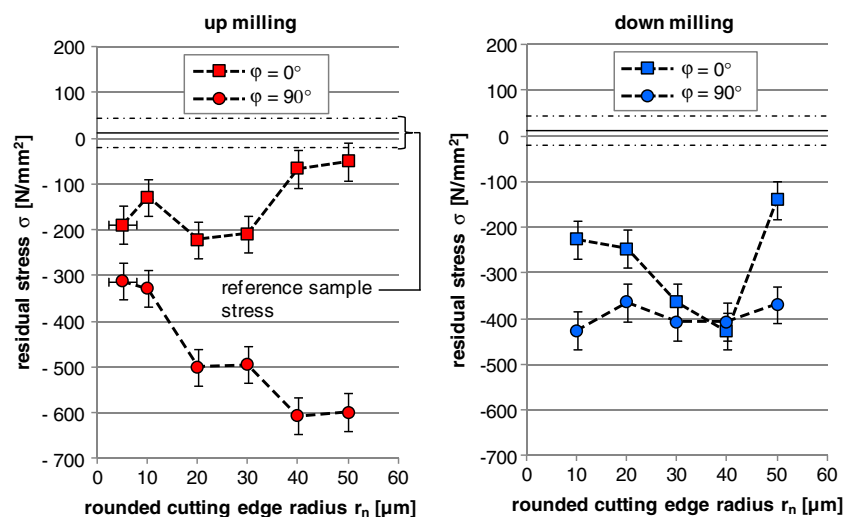
small subsurface areas, this effect might be stronger pronounced than for other metals. However, in up milling, this effect is assumed to have only little influence as a cooled down cutting edge is entering the workpiece. No explanation can be given for the strong variation of the residual stress measured in the direction of cutting ($\varphi=0°$).

4.2 Micro hardness

Hardness is the measure for the resistance of a material against plastic deformation caused by an indenter. Hardness measurements are generally suited for cross-checking the results of residual stress measurements [33]. The higher the compressive stress, the larger is typically the resistance against plastic deformation. The opposite is the case for residual tensile stresses [34, 35].

Vickers hardness measurements were carried out on the identical surfaces as used for the residual stress measurements. At an indentation time of $t_i=20$ s, an indentation force of $F=300$ mN was used. The results are depicted in Fig. 4. Each data point is the average of at least nine measurements randomly distributed over the generated surface.

The polished reference surface has an average hardness of roughly HV420. As expected from the residual stress measurements, the hardness values of milled surfaces are generally higher. The average slope of hardness values against cutting edge radius is in agreement with the maximum compressive residual stresses from the X-ray diffraction measurements in Fig. 3. On the surfaces that were machined by up milling, hardness increases slightly with increasing cutting edge radius, whereas no significant influence of cutting edge radius on hardness was detected on the down milled surfaces. Thus, rounded cutting edges have a positive influence on residual compressive stresses, with a more significant effect in up milling than in down milling.
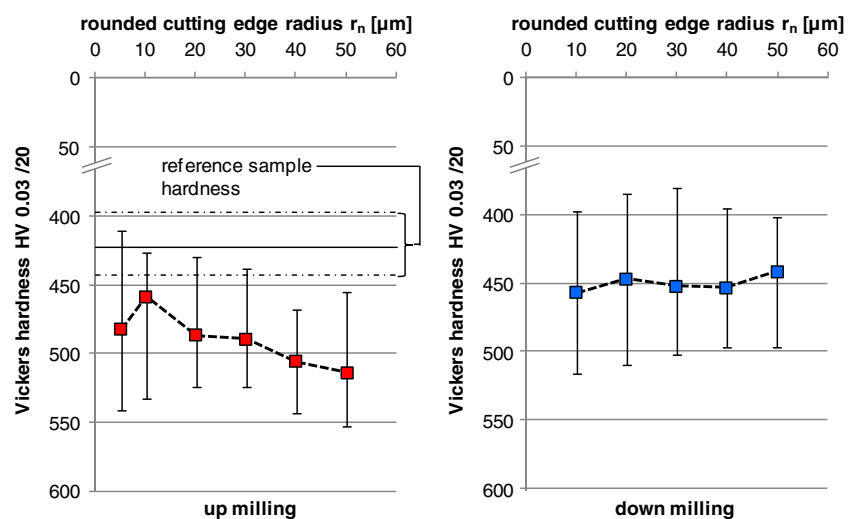
4.3 Surface and near surface characterisation

The effect of the cutting edge radius on surface finish was analysed using scanning electron microscopy. Figure 5 shows images of surfaces generated by up and down milling. Horizontal traces are caused by notchedness of the edge, whereas vertical marks are caused by the tool feed. Independent of process kinematics, feed marks become more pronounced at larger cutting edge radii.

In up milling, the following mechanism is assumed: the feed marks result from elastic material deflections that occur when the cutting edge enters the cut, and successive separation of material at the point when minimum chip thickness is reached. At this point, the chip builds up and is separated by the progressing cutting edge from the elastically and plastically deformed material, which partly springs back after the edge has passed. The larger the cutting edge radius, the later this point is reached. Thus, the feed marks become more pronounced. Moreover, workpiece material which is adhered to the cutting edge is rubbed off at cutting edge re-entry and sticks to the surface produced in the previous cut.

A similar mechanism is proposed in down milling: while cutting, material is continuously being separated from the workpiece surface until the minimum chip thickness is reached. At this point, the chip is torn off from the workpiece surface, leaving a tear-off edge and voids, comparable to those found on fretted surfaces. For both up and down milled surfaces, roughness peaks resulting from uncut material might be rubbed over by the cutting edge and smeared into the surface during the successive rotations of the tool.

Polished and etched cross sections of the subsurface areas of samples machined with different cutting edge radii are presented in Fig. 6. Samples were etched by immersing them for 3.5 min into a mixture of 0.3 ml hydrogen fluoride, 0.5 ml nitric acid and 100 ml water.

Fig. 4 Results of micro hardness measurements on Ti–6Al–4V surfaces machined with different cutting edge radii r_n

**Fig. 5** SEM images of surfaces machined with different cutting edge radii r_n
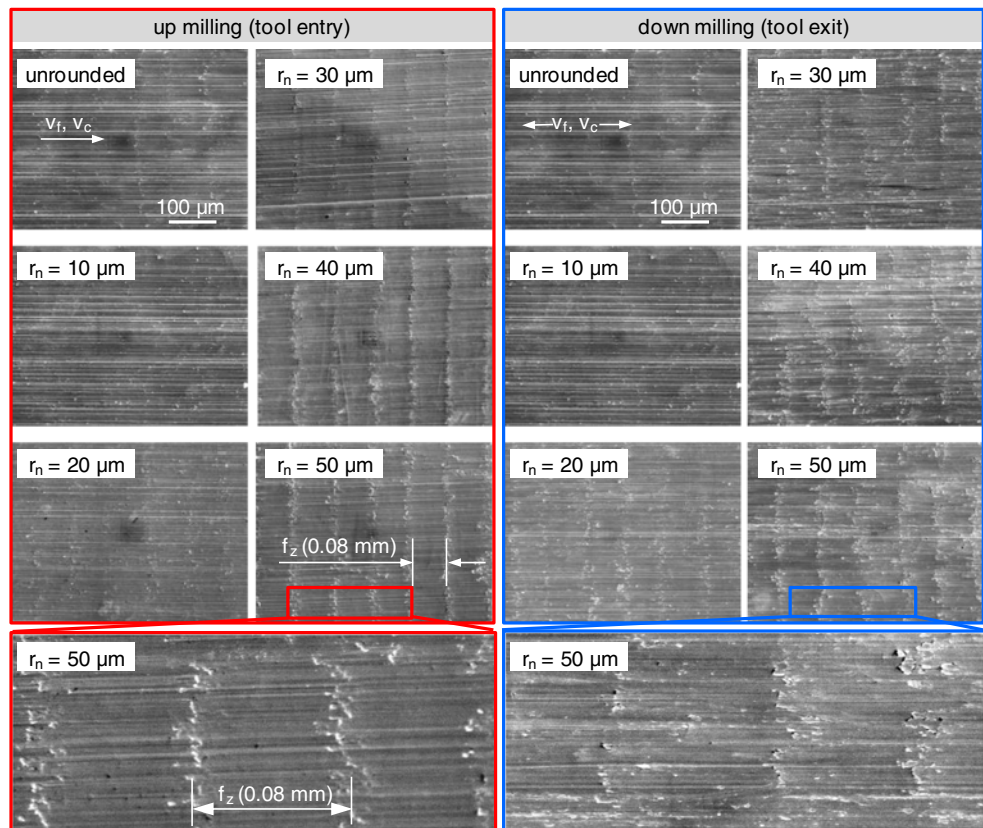
While no noteworthy deformation is visible for surfaces generated with small cutting edge radii, a considerable deformed area can be observed for samples generated with larger cutting edge radii. The maximum visible depth of deformed area approximates 20 μm for a cutting edge radius of $r_n=50$ μm. The findings are thus in agreement with the expected behaviour described above.

4.4 Surface roughness

The theoretical kinematic surface roughness Rz_t in up and down milling can be obtained by

$$Rz_t = \frac{f_z^2}{8 \cdot \left(\frac{1}{2} \cdot d \pm \frac{f_z \cdot n}{\pi}\right)} \approx \frac{f_z^2}{(4 \cdot d)} \tag{1}$$

Fig. 6 Polished and etched cross sections of milled Ti–6Al–4V; the deformed subsurface area increases with increasing cutting edge radius
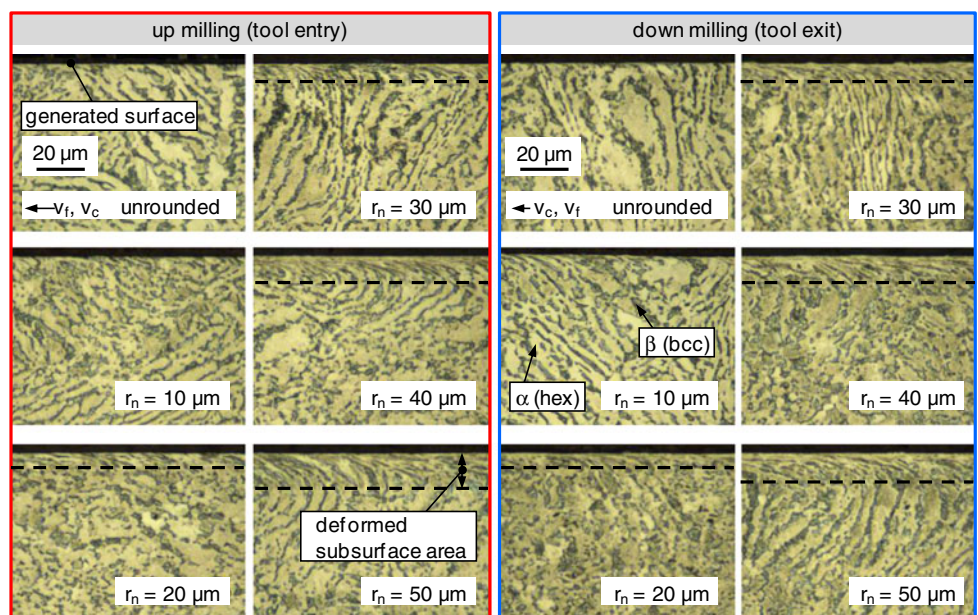
in which f_z is the feed per tooth, n stands for the number of cutting edges and d is the diameter of the cutter [36]. For up milling (+) has to be used, whereas (−) is used for down milling operations. The theoretical arithmetic mean roughness Ra_t can be approximated by [37]:

$$Ra_t \approx 0.064 \cdot \frac{f_z^2}{d} \qquad (2)$$

With a tool diameter of $d=25$ mm and a feed per tooth of $f_z=0.08$ mm, the following roughness values are expected:

$$Rz_t \approx \frac{(0.08 \text{ mm})^2}{100 \text{ mm}} = 0.064 \text{ μm}$$
$$Ra_t \approx 0.064 \cdot \frac{(0.08 \text{ mm})^2}{25 \text{ mm}} = 0.0164 \text{ μm} \qquad (3)$$

The experimentally determined kinematic surface roughness values Ra and Rz are depicted in Fig. 7. Each data point is the average value of nine individual measurements carried out on the surfaces of two different workpieces. The values of Ra and Rz generally lie above the theoretical surface values given in Eq. (3). For both up and down milled surfaces, roughness is minimal when using a rounded cutting edge radius of $r_n=30$ μm. Moreover, the roughness is not in agreement with the visual surface appearance given in Fig. 5, from which an increase in roughness would be expected with increasing edge radius for both up and down milled surfaces.

Unfortunately, Eqs. (1) and (2) only consider the geometrical contact conditions given by tool diameter and feed. According to these equations, the radius of the cutting edge has no influence on the surface roughness. To account for the effect of the cutting edge radius, its impact on elastic deformation before cutting must be taken into account, which influences the minimum uncut chip thickness. [38] stated for turning operations that the achievable surface roughness is influenced by the geometrical contact conditions and the minimum uncut chip thickness h_{min}:

$$Rz_t \approx \frac{f_z^2}{4 \cdot d} + \frac{h_{min}}{2}\left(1 + \frac{d \cdot h_{min}}{2 \cdot f_z^2}\right) \qquad (4)$$

The additional term compensates for residual material that is left on the surface due to under-running the minimum uncut chip thickness. Similar effects are expected at tool entry in up milling, respectively tool exit in down milling. [39] proved the validity of this relation for micromilling.

For the relationship of cutting edge radius r_n and minimum uncut chip thickness, [31] gives the following relationship, without information on workpiece or tool material:

$$h_{min} = 0.293 \cdot r_n \qquad (5)$$

[40] takes the cutting edge radius r_n as well as the friction angle ρ into consideration for determining the minimum uncut chip thickness:

$$h_{min} = r_n\left[1 - \cos\left(\frac{\pi}{4} - \frac{\rho}{2}\right)\right] with \; \rho = \arctan(\mu) \qquad (6)$$

According to Eq. (4), and assuming a linear relation between cutting edge radius and minimum uncut chip thickness, the surface roughness increases by a power law with increasing cutting edge radius. The left side of Fig. 8 shows the theoretical influence of rounded cutting edge radius on achievable surface roughness Rz for the approach given in Eq. (4) and considering different relationships for the minimum uncut chip thickness h_{min}. The influences of constant as well as cutting edge radii-dependent minimum uncut chip thicknesses are depicted. Results that consider Eq. (5) are not shown in Fig. 8 as orthogonal turning tests conducted by the authors with a cutting edge radius of $r_n=50$ μm showed chip formation at an uncut chip thickness of $h=10$ μm. Thus, it can be expected that the ratio of

Fig. 7 Roughness measurements on Ti–6Al–4V surfaces machined with different cutting edge radii r_n
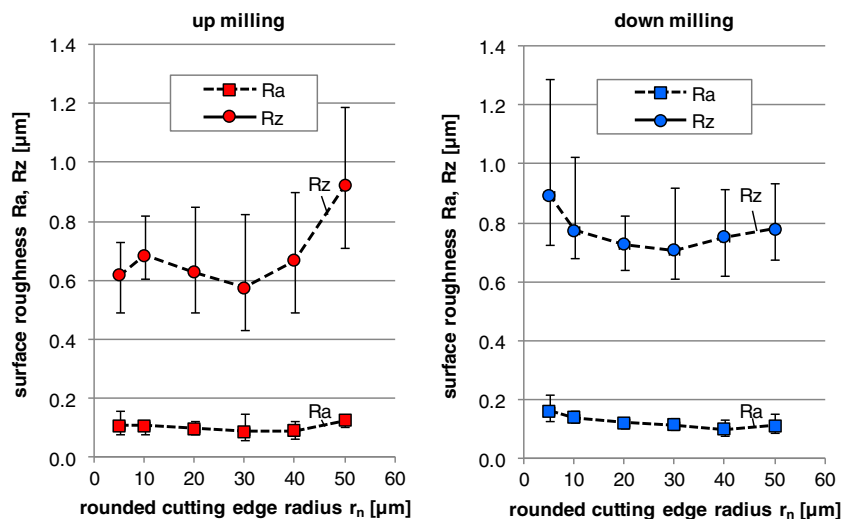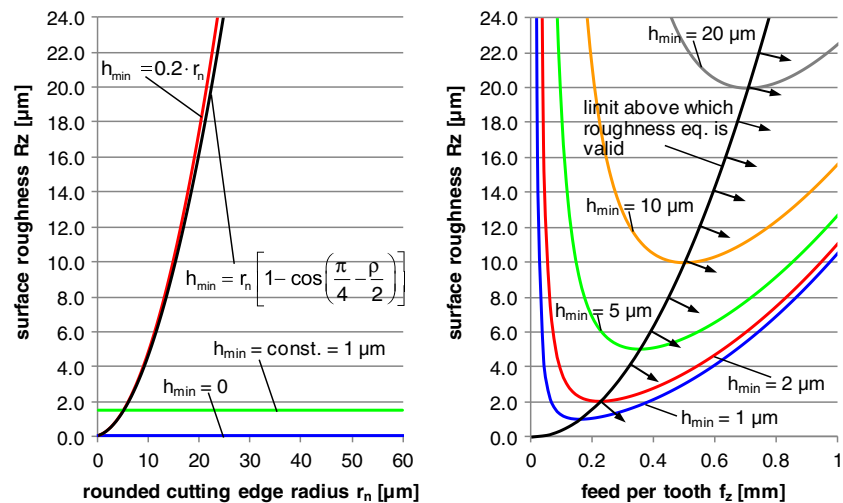
Fig. 8 Theoretical influence of rounded cutting edge radius r_n on achievable surface roughness using different functions for the minimum uncut chip thickness h_{min} (d=25 mm, f_z=0.08 mm) (*left*), influence of feed per tooth f_z on achievable surface roughness considering Eq. (4) and different minimum uncut chip thicknesses h_{min} (d=25 mm) after [38] (*right*)

minimum uncut chip thickness h_{min} to cutting edge radius r_n corresponds to:

$$\frac{h_{min}}{r_n} \leq 0.2 \tag{7}$$

To determine the influence of cutting edge radius on minimum uncut chip thickness with the relation given in Eq. (6), the dependency of the cutting edge radius on average observed friction needs to be known. By using the friction values derived in [3] and a least square algorithm, this relation is linearly approximated to:

$$\mu = 0.0024 \cdot r_n[\mu m] + 0.298 \tag{8}$$

As illustrated on the left side of Fig. 8, the theoretical surface roughness Rz drastically increases when considering minimum uncut chip thickness that depends on the cutting edge radius. This, however, was not observed in the experimental investigations.

The major increase in surface roughness with cutting edge radius is owed to the fact that Eq. (4) is obviously invalid for feed rates which lie below the optimum value f_{min} where a minimum surface roughness is expected. Considering Eq. (4), a tool diameter of d=25 mm and different minimum uncut chip thickness values, the influence of feed per tooth on surface roughness is depicted on the right side of Fig. 8. According to this model, the surface roughness increases drastically at values below the optimum feed per tooth. If the feed per tooth is much smaller than its optimum value (which is the case for the conditions considered), the roughness peaks resulting from uncut material, may on the one hand overlap, and on the other hand, the material residua are plastically deformed during the successive tool revolutions, which in reality causes a surface smoothening [38]. In Eq. (4), these effects are not considered. The feed below which the equation results in a strong increase of

roughness, and can therefore be considered as invalid, is given by [38]:

$$f_{min} = \sqrt{d \cdot h_{min}} \tag{9}$$

Further reasons for a deviation of theoretical and observed surface roughness are tool vibration, material adhesion, as well as workpiece properties, which in turn are influenced by the machining parameters. Therefore, no definite relation can be given for this influence.

Even though the amount of deformed but uncut material between two successive milling cuts increases with increasing cutting edge radius (see Fig. 5), its contribution to the total roughness is insignificant. A general increase in surface roughness with the cutting edge radius was not detected.

4.5 Burr formation

Machining burrs are generally classified by the cutting edge concerned and the mechanism of their formation [41, 42]. In the underlying free orthogonal milling experiments, only the main cutting edge was engaged, producing a sideward burr, also referred to as Poisson burr or top burr [41–43]. The sideward burr is a result of a material's tendency to bulge at the sides when it is compressed until permanent plastic deformation occurs [42]. This tendency is caused by high biaxial compressive stress that pushes material towards the free surface [44]. Burr formation is therefore closely related to the stress state and thus integrity of the generated surface.

The size of burr is a function of the material properties, the effective cutting edge radius and the pressure at the effective radius and flank of the tool. The pressure and thus the tendency to form burr is especially high on materials with low thermal conductivity and low Young's modulus [42]. Both are properties that titanium and its alloys are known for.

[42] compares the effect of the cutting edge radius to a thin cylinder pushed into the workpiece. Bulging occurs at the ends of this cylinder, resulting in burr. The effect increases with increasing cutting edge radius.

Figure 9 depicts surfaces and resulting burr in milling titanium with different cutting edge radii. The left side shows surfaces generated by up milling. The right side shows down milled surfaces. Burr formation occurs on both top and bottom edge as the surfaces were generated in free orthogonal milling.

The burr produced in up milling is frayed (ruptured type). This results from the repeated entrance of the cutting edge into the workpiece. Every time the cutting edge enters the cut, new material is bulged at the free surfaces, pushing out the burr from the previous cut. On the one hand, this leads to an increase in burr height. On the other hand, it causes a partial separation of burr from the machined edge. Below a certain cutting edge radius, it can be assumed that burr of the previous cut is partly removed by the successive cut. With increasing cutting edge radius, however, the burr formed at the beginning of chip formation is not removed by a successive cut, but only pushed away, leading to burr with long fringes. Especially for cutting edge radii of $r_n=40$ μm or larger, this effect seems to take place.

In down milling, no significant burr formation was observed for cutting edge radii of $r_n=10$ μm or smaller. As expected, burr formation increased when the cutting edge radius became larger. The burr formation is generally much more pronounced in up milling than in down milling.

Burr formed in up milling is generated before chip formation occurs or at the onset of chip formation respectively, whereas in down milling, burr is generated at the separation of the chip from the surface. This causes the burr to be removed with the chip. In most cases, only the root of the burr remained on the machined edge, resulting in a rather small and uniform burr in down milling when compared to the one produced in up milling. Nevertheless, an increase of burr with increasing cutting edge radius was also observed in down milling. Thus, the increase in burr with increasing cutting edge radius is generally in agreement with the measurement results of residual stress of machined surfaces.

5 Summary and conclusions

To understand the influence of the cutting edge radius on surface integrity in milling Ti–6Al–4V, slot milling tests were carried out with different cutting edge radii. The tests exhibit high residual stresses of compressive type, which are generally favourable for fatigue properties of workpieces. In up milling, the compressive residual stresses increase with the cutting edge radius, whereas no uniform trend was observed in down milling. The difference in up and down milling is potentially caused by the influences of process kinematics and cutting temperature. Experiments focusing on the effect of the cutting edge radius on cutting temperature could help to further explain the effects observed. Since the cutting temperature is assumed to cause differences in the surface stress state, the results may change when using for example different cutting speeds, cutting materials or coolant conditions. To separate the individual influences, further analyses are required.

In this experimental study, the residual stress measurement results were cross-checked and verified by micro hardness indentation tests. Cross sections of surfaces generated by up and down milling revealed an increase in plastically deformed surface layer with increasing cutting edge radius.

Fig. 9 Burr formation when milling Ti–6Al–4V with different cutting edge radii r_n, (v_c=70 m/min, f_z=0.08 mm, a_e=d=25 mm)
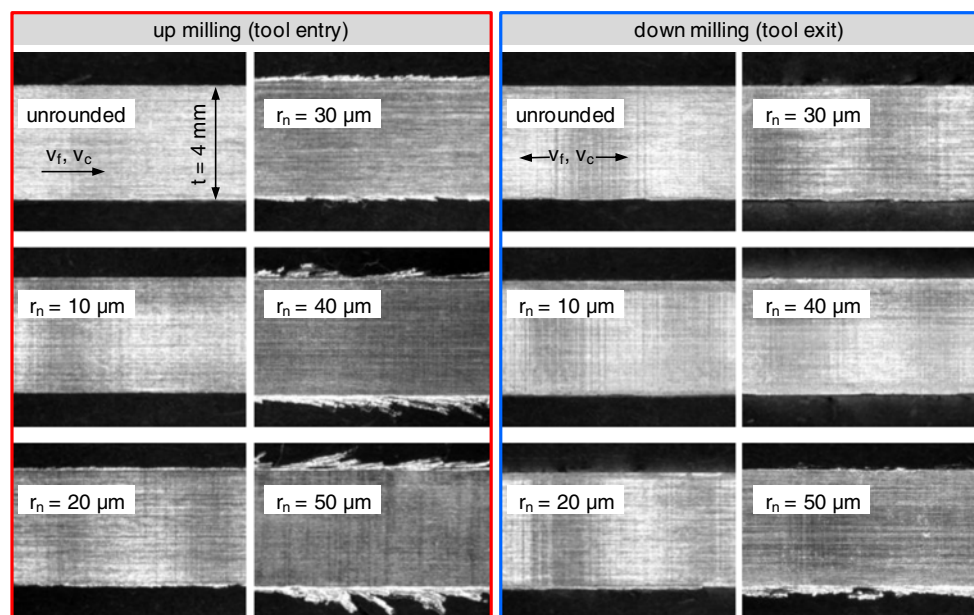
The roughness is not uniformly influenced by the cutting edge radius.

The positive influence of the cutting edge radius on compressive residual surface stress comes with a negative influence on burr formation, which is caused by strong plastic deformation of material in front of the cutting edge. The formation of burr is thus in agreement with the residual stress measurements. Burr formation increases with the cutting edge radius and is especially pronounced in up milling. It is less pronounced in down milling as burr is partly removed with the chip.

The results of these experiments can be specifically used to improve the quality of the machined surface. Especially in aerospace applications, where the integrity of the machined surface often is of major importance, or also in high precision machining applications the results give a further decision basis for selecting the right process conditions.

References

1. Biermann D, Terwey I (2008) Cutting edge preparation to improve drilling tools for HPC processes. CIRP J Manuf Sci Technol 1 (2):76–80
2. Terwey I (2008) *Leistungssteigerung bei Zerspanwerkzeugen durch Kantenpräparation. Zerspanen im modernen Produktionsprozess*, Fachgespräch zwischen Industrie und Hochschule, 26.2.-27.2. 2008, Dortmund (eds. K. Weinert, D. Biermann)
3. Wyen C, Wegener K (2010) Influence of cutting edge radius on cutting forces in machining titanium. Ann CIRP 59(1):93–96
4. Ozturk S, Altan E (2012) A slip-line approach to the machining with rounded-edge tool. Int J Adv Manuf Technol, pp. 1–10. doi:10.1007/s00170-012-3941-6
5. Outeiro JC (2010) Size-effects and surface integrity in machining and their influence on product sustainability. Int J Sustain Manuf 2 (1):113–126
6. Rech J (2006) Influence of cutting edge preparation on the wear resistance in high speed dry gear hobbing. Wear 261:505–512
7. Cortés Rodríguez CJ (2009) Cutting edge preparation of precision cutting tools by applying micro- abrasive jet machining and brushing. Dissertation, Kassel University
8. Wang X, Huang C, Zou B, Liu H, Wang J (2012) Effects of geometric structure of twist drill bits and cutting condition on tool life in drilling 42CrMo ultrahigh-strength steel. Int J Adv Manuf Technol. doi:10.1007/s00170-012-4026-2
9. Elsharkawy M (1975) Einfluss des Ecken- und Schneidkantenradius auf die Oberflächengüte beim Feindrehen. Fertigungstechnik Betrieb 25(4):230–233
10. Betz F (1971) Untersuchungen zur Entstehung der Schnittflächenrauheit bei der spanenden Bearbeitung. Dissertation, ETH Zurich
11. Kötter D (2006) Herstellung von Schneidkantenverrungdungen und deren Einfluss auf das Einsatzverhalten von Zerspanwerkzeugen. Dissertation, Dortmund University
12. Byelyayev O (2008) Erhöhung der Leistungsfähigkeit von HSS-Spiralbohrern durch Einsatz der magnetabrasiven Bearbeitung. Dissertation, Technical University Magdeburg
13. Xu G (1996) Einfluss der Schneidkantenform auf die Oberflächenausbildung beim Hochgeschwindigkeitsfräsen mit Feinkornhartmetall. Dissertation, TU Darmstadt
14. Weinert K, Kötter D, Kresing I (2006) Präparierte Werkzeugschneidkanten optimieren das Schnittverhalten. MM Maschinenmarkt 50:22–25
15. Denkena B, Friemuth T, Spengler C, Weinert K, Schulte M, Kötter D (2003) Kantenpräparation an Hartmetall-Werkzeugen. wt Werkstatttechnik online 93(3):202–207
16. Kreis W (1973) Verschleissursachen beim Drehen von Titanwerkstoffen. Dissertation, RWTH Aachen Technical University
17. Altmüller S (2000) Simultanes fünfachsiges Fräsen von Freiformflächen aus Titan. Dissertation, RWTH Aachen Technical University
18. Field M, Kahles JF (1964) The surface integrity of machined and ground high strength steels. DMIC Report 210:54–77
19. Stephenson DA, Agapiou JS (2006) Metal cutting theory and practice. CRC Press, Boca Raton
20. Lucca DA, Brinksmeier E (1998) Progress in assessing surface and subsurface integrity. Ann CIRP 47(2):669–693
21. Wyen C, Wegener K (2010) Experimental study of micro abrasive jet machining for the generation of rounded cutting edges on cemented carbide tools. 8th International Conference on High Speed Machining, Metz, France, pp. 367–373
22. Wyen C, Wegener K (2011) A new method for the characterisation of rounded cutting edges. Int J Adv Manuf Technol 59(9–12):899–914
23. Eigenmann B, Macherauch E (1995) Röntgenographische untersuchung von spannungszuständen in werkstoffen–Teil III. Matwiss Werkst 27:426–437
24. Birkholz M (2006) Thin film analysis by X-ray scattering. Wiley, Weinheim
25. Prevéy PS (1986) X-ray diffraction residual stress techniques In: Metals handbook. American Society for Metals, Metals Park, pp. 380–392
26. Noyan IC, Cohen JB (1987) Residual stress—measurement by diffraction and interpretation. Springer, New York, pp 164–210
27. DIN EN ISO 4288 (1998–04) Geometrische Produktspezifikation (GPS)-Oberflächenbeschaffenheit: Tastschnittverfahren-Regeln und Verfahren für die Beurteilung der Oberflächenbeschaffenheit. German Institute for Standardization, Berlin
28. Davim JP (2010) Surface integrity in machining. Springer, London
29. Albrecht P (1960) New developments in the theory of the metalcutting process. Part 1: the ploughing process in metal cutting. ASME J Eng Ind 81:348–358
30. Scholtes B (1990) Eigenspannungen in mechanisch randschichtverformten Werkstoffzuständen, Ursachen, Ermittlung und Bewertung, Habilitation, TH Karlsruhe
31. L'VOV NP (1969) Determining the minimum possible chipthickness. Mach Tool 40(4):45–46
32. Denkena B, de León-García L, Köhler J (2005) *Bearbeitungsinduzierte Eigenspannungen beim Fräsen von Aluminium und Titan*, Neue Fertigungstechnologien in der Luft- und Raumfahrt, Seminar, Hannover (23–24 November)
33. Klein H-D (1969) Eigenspannungen und ihre Verminderung in metallischen Werkstücken durch spanende Bearbeitung. Dissertation, TU Hannover
34. Tosha K (2002) Influence of residual stresses on the hardness number in the affected layer produced by shot peening. 2nd Asia-Pacific Forum on Precision Surface Machining and Deburring Technology, Seoul, Korea (July) pp. 48–54
35. Frankel J, Abbate A, Scholz W (1993) The effect of residual stresses on hardness measurements. Exp Mech 33(2):164–168
36. Martellot M (1941) Analysis of the milling process. Trans ASME 63:677–700

37. Qu J, Shih AJ (2003) Analytical surface roughness parameters of a theoretical profile consisting of elliptical arcs. Mach Sci Technol 7 (2):281–294

38. Brammertz PH (1961) Die entstehung der oberflächenrauheit beim feindrehen. Ind-Anz 2:25–32

39. Weule H, Hüntrup V, Tritschler H (2001) Micro-cutting of steel to meet new requirements in miniaturization. Ann CIRP 50(1):61–64

40. Son SM, Lim HS, Ahn JH (2009) Effects of the friction coefficient on the minimum cutting thickness in micro cutting. Int J Mach Tool Manuf 45:529–535

41. Nakayama K, Arai M (1987) Burr formation in metal cutting. Ann CIRP 36(1):33–36

42. Gillespie LK, Blotter PT (1976) The formation and properties of machining burrs. Trans ASME, J Eng Ind 98:66–74

43. Hashimura M, Hassamontr J, Dornfeld DA (1999) Effect of in-plane exit angle and rake angles on burr height and thickness in face milling operation. Trans ASME, J Manuf Sci Eng 121 (February):13–19

44. D. Dornfeld, S. Min (2010) A review of burr formation in machining. In: Burrs—analysis, control and removal. Springer, Berlin, pp. 3–11

45. Rangaswamy P, Prime MB, Daymond M, Bourke M, Clausen B, Choo H, Jayaraman N (1999) Comparison of residual strains measured by X-ray and neutron diffraction in a titanium (Ti-6Al-4V) matrix composite. Mater Sci Eng A259:209–219

46. Halevy I, Zamir G, Winterrose M, Sanjit G, Grandini CR, Moreno-Gobbi A (2010) Crystallographic structure of Ti-6Al-4V, Ti-HP and Ti-CP under high-pressure. J Phys Conf Ser 215:012013